PUBLISHED BY INSTITUTE OF PHYSICS PUBLISHING

Journal of Physics: Condensed Matter

Top Papers 2005 Showcase highlights the leading and most frequently downloaded papers, letters and topical reviews from Journal of Physics: Condensed Matter, arguably the world's most authoritative source of topical information for condensed matter physicists and materials and surface scientists. Journal of Physics: Condensed Matter covers experimental and theoretical studies of the structural, thermal, mechanical, electrical, magnetic and optical properties of condensed matter and is published 50 times per year by Institute of Physics Publishing.

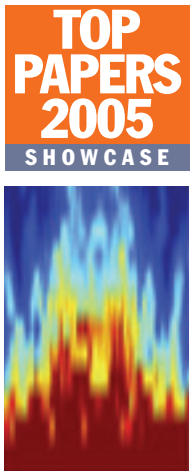

We welcome papers and submissions from authors who have research interests in these areas. Authors can benefit from rapid receipt-to-publication times, a rising impact factor and a large and growing world wide readership both in print and on-line. On average papers are downloaded on-line over 100 times via our award winning Electronic Journals service.

For more information on the submission process and to view the latest published papers from Journal of Physics: Condensed Matter visit **www.iop.org/EJ/journal/JPhysCM**

PAPERS

REVIEW ARTICLES

Inside you will find synopses of all the top papers and reviews listed above, together with details of where to find the full articles ➔➔➔➔

Ultrahydrophobic surfaces

Towards ultrahydrophobic surfaces: a biomimetic approach
Ulrike Mock, Ralf Förster, Wolfgang Menz and Jürgen Rühe
J. Phys.: Condens. Matter
17 (2005) S639–S648

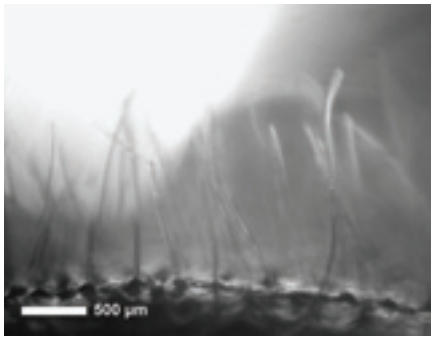

Optical micrograph of the hydrophobic polyether structure that was obtained by remoulding of the silicone elastomer, which was the direct mould of the lady's mantle leaf.

Many biological surfaces, particularly plant leaves, are hydrophobic. As strongly water-repellent and self-cleaning surfaces are very interesting technologically, many approaches to ultrahydrophobic surfaces have been developed. One such plant is the lady's mantle, whose leaves are covered with hairs, which apparently help make it ultrahydrophobic. This is surprising as simple theories of wetting on a rough substrate predict that a rough hydrophilic surface should be even more hydrophilic than a smooth one. Herminghaus *et al* proposed that the elasticity of the plant hair as well as its area coverage accounts for the water repellence of such hairy leaves.

Jürgen Rühe and colleagues at University of Freiburg, Germany, studied a model surface closely resembling the leaf surface of a lady's mantle. They used a three-step approach to obtain elastic hydrogel pillars as models for such hairy plant surfaces. They first generated master structures either in steel or through the direct replication of the leaf surface in polymer. This master was moulded against a silicone polymer to yield an elastomer which was a negative of the hairy surface. A subsequent radical polymerization under crosslinking in the negative led to the formation of an elastic hydrogel resembling the natural structure. The hydrogels obtained were hydrophilic, had aspect ratios from four up to 100 as in the natural system and showed elastic properties, so that bundle formation of several pillars could be observed. These models mimic roughly the structure of the leaf of a lady's mantle.

In further experiments they will concentrate on the choice of appropriate polymers with suitable swelling behaviour and elastic properties. The crosslink density of the polymer networks needs to be controlled and an appropriate choice of the chemical composition of the network-building components will have a great influence on the wetting properties of the resulting hairy surface.

High-energy photoemission in silver

High-energy photoemission in silver: resolving d and sp contributions in valence band spectra
G Panaccione, G Cautero, M Cautero, A Fondacaro, M Grioni, P Lacovig, G Monaco, F Offi, G Paolicelli, M Sacchi, N Stojic, G Stefani, R Tommasini and P Torelli
J. Phys.: Condens. Matter
17 (2005) 2671–2679

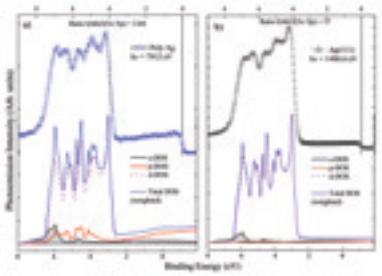

Measured valence band spectra of polycrystalline Ag (left) and Ag(111) (right), compared with the total weighted DOS. The partial s, p, d DOSs are also shown. The vertical lines indicate the Fermi levels of the experimental spectra. Calculated DOSs have been arbitrarily shifted for comparison.

Low-energy angle-resolved photoemission spectroscopy (PES), in the UV and soft x-ray range, provides detailed information on electronic states, with a strong surface sensitivity. At higher photon energies, x-ray photoelectron spectroscopy (XPS) increases the probing depth. Hard x-ray PES (HAXPES) offers a more detailed insight, but these experiments are difficult, and very weak signals are expected as the photoionization cross section decreases as E^{-3}. High-flux/high-resolution beamlines at third-generation synchrotron radiation sources and recent advances in analyser technology have made HAXPES viable.

G Panaccione (Trieste) and co-workers have obtained high-resolution core level and valence band HAXPES spectra from polycrystalline Ag to (i) compare HAXPES results with standard XPS spectra and with bulk-DOS calculations, and (ii) try to separate the 4d and sp contributions in valence band PES. The weak surface contribution to their spectra permits a simple comparison with the calculated bulk DOS.

The 3d and valence band HAXPES spectra of polycrystalline Ag display larger bulk sensitivity and improved energy resolution than standard XPS. The surface signal is negligible (less than 3%). HAXPES valence band spectra can be compared with calculated bulk DOS, ignoring the surface contribution. By optimizing the weight of the calculated s, p and d DOSs to match valence band spectra measured at different photon energies, they found a reduced I(4d)/(I(5s) + I(5p)) ratio compared with calculated values, namely ~40 instead of ~70 for XPS and 2.8 instead of 7 at $h\nu = 7912$ eV. This enables HAXPES spectra to yield a more accurate picture of the Ag valence band. The 5p-band is responsible for the observed increase of the intensity approaching the Fermi level and has the strongest free-electron-like character, whereas localized s-states are present at the bottom of the d-band.

This technique may be extended to other materials. Comparing DOS calculations with HAXPES data and exploiting the behaviour of photoelectron cross-sections at high kinetic energy will enable the electronic properties of complex systems like transition metal oxides to be studied. Despite the challenging experimental conditions of HAXPES, they anticipate applications to samples of technological interest, thanks to the more relaxed vacuum and surface preparation requirements.

Opening up photonic bandgaps

Opening up complete photonic bandgaps by tuning the orientation of birefringent dielectric spheres in three-dimensional photonic crystals
Fang Guan, Zhifang Lin and Jian Zi
J. Phys.: Condens. Matter
17 (2005) L343–L349

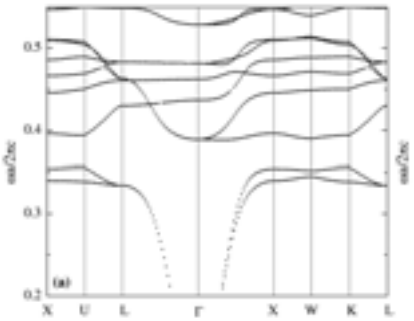

Calculated photonic band structures of a PC consisting of Te spheres in the fcc lattice with filling fraction 0.3. The extraordinary axis of Te spheres is oriented along [111]. A PBG between the second and third photonic bands can be seen with midgap ratio $-\omega/\omega_g = 5.6\%$. and a small PBG between the eighth and ninth photonic bands with $-\omega/\omega_g = 0.84\%$.

Photonic crystals are composite structures with a spatially periodic variation of refractive index. Light propagation in them can be strongly modulated not only by the introduced periodicity via multiple Bragg scattering but also by the presence of resonant modes of the building components and is then characterized by complicated photonic band structures. If there exist complete photonic bandgaps between photonic bands, light propagation will be absolutely forbidden and spontaneous emission prohibited within the frequency range of the photonic bandgap, giving rise to unprecedented degrees of freedom in the manipulation and control of spontaneous emission as well as light propagation, leading to many potential applications in photonics, such as frequency selective reflectors, band filters, and low threshold micro-cavity lasers.

Fang Guan, Zhifang Lin and Jian Zi of Fudan University, Shanghai have used a multiple-scattering method to study the photonic band structures of three-dimensional photonic crystals consisting of birefringent dielectric spheres. In the multiple-scattering method the whole system is treated as an assembly of scatterers and its scattering properties are taken as sums over individual scatterers. Once the scattering properties of the individual scatterers are characterized by the scattering matrix (or scattering coefficients for an isotropic sphere), the scattering properties of the entire system can be constructed and the band structure of the photonic crystals can be obtained from the stationary-state solution of the systems.

Their results demonstrate the possibility of opening up complete photonic bandgaps in simple three-dimensional lattice photonic systems by changing the orientation of the extraordinary axis of the birefringent spheres. The creation of the complete photonic bandgaps in the photonic crystals also suggests some degree of tunability of the photonic band structure, provided that the extraordinary axis of all constituent birefringent spheres can be rotated while keeping the whole structure of the photonic system unchanged. The application of a strong external electric field may be a handle to achieve this tunability.

A 'magnetic' interatomic potential

A 'magnetic' interatomic potential for molecular dynamics simulations
S L Dudarev and P M Derlet
J. Phys.: Condens. Matter
17 (2005) 7097–7118

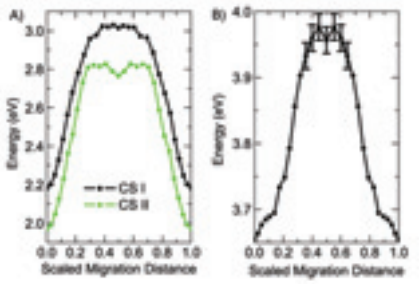

(A) Vacancy migration energy curves for two case studies I and II. (B) (110) self-interstitial migration energy curve for case study II showing double-hump structure.

Predictive models of iron-based alloys and steels for fusion and advanced nuclear applications must take into account magnetic effects to obtain accurate models of interatomic interactions. It is known that magnetism makes the BCC α-phase of iron more stable than any of the FCC phases, possibly through the effect of electron correlations on interatomic forces. The density functional and tight-binding approaches cannot model systems containing ~100 000 atoms, necessary to account for the long-range elastic interactions causing swelling, embrittlement and creep of irradiated materials. Phenomenological models suitable for fast evaluation of forces between atoms in a magnetic material are required for molecular dynamics simulations of thermally activated processes in irradiated iron and its alloys.

S L Dudarev (Culham) and P M Derlet (Paul Scherrer Institute) have developed such a model combining the Stoner and Ginzburg–Landau (GL) models. The Stoner model describes correlation effects giving rise to magnetism in an electron gas, while GL is the simplest model of a second-order phase transition. They show that the symmetry-broken solutions of the GL model describing spontaneous magnetization of atoms cause the link between magnetism and interatomic forces.

They derive a phenomenological embedding function of the many-body interatomic potential. By adjusting the effective pairwise density functions and pairwise interactions they parameterize the energy of interatomic interactions to describe the equation of state both for the non-magnetic and magnetic configurations, and also the energies of vacancy and self-interstitial point defects in α-iron.

They extend the existing treatment of interatomic interactions, where the energy is a single-valued function of atomic coordinates, and link it with symmetry breaking, leading to multi-branching of the effective potential. Since in a magnetic system the energy depends on both the position of atoms and the configuration of magnetic moments, the total energy is no longer a unique function of atomic coordinates. Instead, in a magnetic system they find that several energy surfaces correspond to the same geometric configuration of atoms. They treat only the ferromagnetic case where the energy surface consists of two (non-magnetic and ferromagnetic) sheets, but the method can be generalized to arbitrary magnetic configurations.

Birth, death and diffusion

Birth, death and diffusion of interacting particles
Emilio Hernández-García and Cristóbal López
J. Phys.: Condens. Matter
17 (2005) S4263–S4274

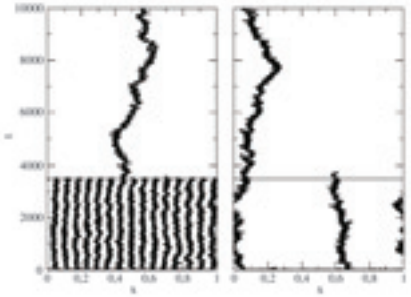

Left: evolution of a set of 15 clusters prepared under $R = 0.05$ before we change R to global coupling $R = L/2$ at time $t_i = 3500$ (indicated by the horizontal line). A short time afterwards, a single cluster survives. Right : analogous simulation but with only two clusters (prepared under $R = 0.324$) before switching to global coupling at $t_i = 3500$.

Interacting particle systems are models in which individual particles evolve in time following microscopic rules, from which collective macroscopic behaviour may emerge. They are used to model physical, chemical, social, and biological dynamics. If birth and death processes occur, the combination of this number-changing dynamics with the diffusive motion leads to the formation of clusters and the apparent attraction among individuals that are actually non-interacting.

Emilio Hernández-García and Cristóbal López of the University of the Balearics have previously considered the case of a birth rate which is reduced proportionally to the number of particles at a distance smaller than a range R. In a biological setting this models in a natural way competition for resources, but it can also be a consequence of other phenomena such as toxin production. The most notable effect of the interaction was the appearance of a clustering instability organizing the distribution of individuals into clusters separated by a typical distance.

In the present paper they focus on such coherent objects, the clusters and analyse their diffusive motion, their size, and some aspects of their dynamics and interactions. The situation in which the range of interaction is of the order of the system size, so that any individual interacts with all the others in the system, allows them to focus on the dynamics of a single cluster: under these conditions a permanent unique cluster emerges in the system which helps to understand and characterize the clustering dynamics of the model. Note that a coarse-grained deterministic description of the system cannot explain the appearance of the cluster in this limit of global interaction of particles, placing emphasis on the importance of the fluctuations (discrete nature of the particles) in the model. The paper derives expressions for lifetimes, sizes, and collective diffusion that agree very well with numerical simulations.

Universal features of localization

Universal features of localized eigenstates in disordered systems
J J Ludlam, S N Taraskin, S R Elliott and D A Drabold
J. Phys.: Condens. Matter
17 (2005) L321–L327

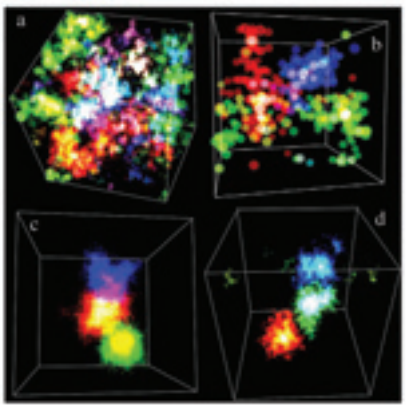

Universality of localized-eigenstate structure for sets of three localized eigenstates (red, green and blue) for various systems, showing spatial overlap of islands. (a) Three adjacent-energy eigenvectors taken from the band centre for the electronic Anderson model on a simple cubic lattice with the critical ratio of the range of on-site disorder of width W to the off-diagonal interaction, V, i.e. $W/V = 16.5$, sufficient to localize all states in the band. These are critical eigenvectors of the model, and are clearly constructed from islands. The appearance of the same islands in consecutive eigenstates is clearly evident. (b) Three adjacent-energy vibrational eigenvectors of a 1650-atom vitreous silica model. Three regions, that are mainly red, green and blue, can be seen, and each of these has a white centre, indicating overlap of the three eigenvectors at these points. (c) Three adjacent-energy vibrational eigenvectors on a 48-site FCC lattice with force constants taken from a uniform distribution of width 2.0 and average value 1.0 (the crystal has a force-constant value of unity). The overlapping island states are less isotropic because of the underlying lattice. (d) Three adjacent-energy vibrational eigenvectors (red, green, blue) of a 10 000-atom model of a-Si, again showing strongly overlapping islands.

In crystalline materials, electronic (and vibrational) eigenstates are extended (or delocalized) throughout the material, but disorder can cause some electron states to decay exponentially in space. This is known as 'localization', and is usually studied by the 'Anderson model'.

Localization–delocalization transitions occur in problems ranging from semiconductor-device physics to propagation of disease in plants and viruses on the internet. D A Drabold (Ohio) and S R Elliott and co-workers (Cambridge) report calculations of localized electronic and vibrational eigenstates for remarkably different, mostly realistic, disordered systems and point out similar characteristics among them. They show in each case that the eigenstates may be decomposed into exponentially localized islands of 'charge' (electron probability density, vibrational displacement field) which may appear in many different eigenstates. These individual islands spatially decay exponentially and their localization length does not change dramatically near the localization–delocalization transition. The number of islands reaches a value consistent with the space-filling nature of extended states around the localization–delocalization transition, thus producing a connectivity of the excitations (electronic or vibrational) through the system, being conceptually akin to a percolation model at criticality. They show that consistent island extraction is possible for all these systems.

Dephasing in open quantum-dot arrays

Dephasing due to coupling to the external environment in open quantum-dot arrays

M Elhassan, J P Bird, R Akis, D K Ferry, T Ida and K Ishibashi

J. Phys.: Condens. Matter
17 (2005) L351–L357

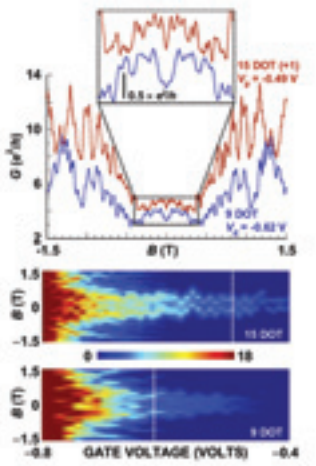

Top: magnetoconductance fluctuations in the 9- and 15-dot arrays. Lower: magnetoresistance contours for the 9- and 15-dot arrays. The dotted lines indicate the gate voltage values corresponding to the two traces in the upper panel. All measurements were made at a cryostat temperature of 0.02 K.

Electron dephasing determines the extent to which mesoscopic systems are influenced by quantum interference, and arises from interaction with their environment. In disordered systems this interaction arises mainly from electron–phonon and electron–electron scattering, which are weak at low temperatures, so coherent quantum interference effects, such as weak localization and universal conductance fluctuations, can be observed in the conductance, but these quantum phenomena are suppressed at higher temperatures.

Quantum interference is important in semiconductor quantum dots, in which electrons move ballistically within the dot while large-angle scattering occurs mainly at its boundaries. Dephasing in quantum dots might be expected to arise predominantly from their interaction with their external reservoirs, rather than from the internal electronic dynamics, and it has been argued theoretically that intra-dot interactions do not give rise to dephasing, while experiments have shown that the dephasing time in open dots can be strongly affected by their coupling to the reservoirs.

David Ferry of Arizona State University and co-workers have investigated dephasing due to the external environment by studying the scaling characteristics of quantum interference in linear arrays of coupled quantum dots. They analysed the amplitude of the fluctuations in the low-temperature magnetoconductance, which provide a sensitive indicator of quantum coherence. Their key result is the discovery of a common scaling behaviour, according to which the fluctuation amplitude varies in direct proportion to the total conductance of the system, independently of the size of the arrays. They argue that such behaviour is inconsistent with a classical scaling of incoherently coupled dots, but is reasonable for that expected when dephasing arises from the interaction of the quantum system with its external environment. On the basis of these results, they believe that much still needs to be done to understand the origins of dephasing in open, but strongly quantized, systems.

Raman study of carbon substituted MgB_2

Raman scattering investigation of electron–phonon coupling in carbon substituted MgB_2

T Sakuntala, A Bharathi, S K Deb, N Gayathri, C S Sundar and Y Hariharan

J. Phys.: Condens. Matter
17 (2005) 3285–3292

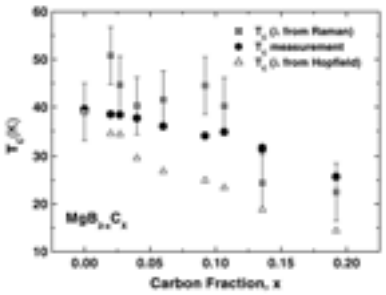

T_C dependence on x in $MgB_{2-x}C_x$ calculated from the λ_{2g} variation obtained from Raman data, and from the Hopfield expression. The experimentally measured T_C is also shown for comparison.

The discovery of superconductivity at 39 K in MgB_2 has attracted much attention because of the unusual two-gap nature of superconductivity in this system and also because of the possibility of attaining high critical fields. Carbon substitution reduces T_C but increases the critical field. The T_C of MgB_2 with ~10 at.% of the B substituted with carbon is 22 K. This decrease in T_C is much smaller than that expected from rigid band behaviour. Band structure calculations indicate that for $x = 0.2$ the σ-band holes are still present and for $x = 0.4$ they completely vanish at E_F. It is also suggested that the electron–phonon coupling strength mediated by the E_{2g} bond-stretching mode should increase substantially for small C substitutions.

This E_{2g} mode is Raman active and couples strongly with the σ-band holes leading to the high T_C of MgB_2, so Raman scattering helps in understanding superconductivity in MgB_2. The E_{2g} mode in MgB2 is at ~600 cm^{-1}, much lower than the 980 cm^{-1} of the isostructural, non-superconducting AlB_2. This is largely due to electron–phonon coupling.

A Bharathi and colleagues at the Indira Gandhi and Bhabha Atomic Research Centres have studied the evolution of the E_{2g} phonon with C substitution in $MgB_{2-x}C_x$ for a wide range of composition. From the observed frequency and the linewidth variations of the Raman shift, and the calculated σ-hole density of states, they evaluated the e–p coupling strength as a function of carbon fraction.

They performed room-temperature Raman scattering measurements in $MgB_{2-x}C_x$ samples with $x = 0.0$–0.2. The average phonon frequency increased with C substitution, whereas the linewidth increased to a maximum for $x = 0.1$ and then decreased. They calculated the electron–E_{2g} phonon interaction parameter λ_{2g} using Allen's formula. Its value in pristine MgB_2 was in good agreement with that obtained from x-ray inelastic scattering. By suitably incorporating the $\lambda_{2g}(x)$ variation in λ_{tot} appearing in McMillan's equation, they found that the variation of $T_C(x)$ compared well with the measured value.

Dewetting of polymer films

Dynamics and structure formation in thin polymer melt films

Ralf Seemann, Stephan Herminghaus, Chiara Neto, Stefan Schlagowski, Daniel Podzimek, RenateKonrad, Hubert Mantz and Karin Jacobs

J. Phys.: Condens. Matter
17 (2005) S267–S290

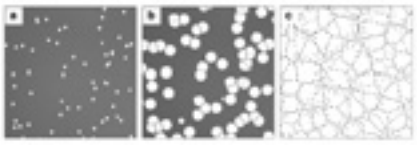

Pictures taken by a light microscope: 80 nm thick polystyrene film of 65 kg mol^{-1} molecular weight is dewetting at 135°C from a hydrophobized silicon substrate. (a) t = 2 min, (b) t = 18 min, (c) t = 100 min.

Thin liquid films on solid surfaces are important in everyday life as lubricants, as coatings, e.g. to protect hardware from rust, to colour surfaces, or to change the wetting properties of substrates. In all these examples it is essential that the liquid wets the substrate: only then can a homogeneous film be achieved. So it is important to understand the origin of dewetting.

Karin Jacobs at Saarland University and co-workers have studied the stability of thin liquid films on solid surfaces. A detailed analysis of the structures that emerge in dewetting has led to a comprehensive picture of thin film stability. They distinguished experimentally three different pathways of dewetting (spinodal, homogeneous and heterogeneous) that were expected theoretically. Studies on spinodally dewetting films allowed them to derive the effective interface potential. Additive van der Waals forces were adequate for correctly describing the potential. Experiments recording the dynamics of dewetting gave insight into the viscosity of a thin film. They demonstrated that thin films of polystyrene below the entanglement length also exhibit a reduction of the glass transition temperature. A new theoretical approach was required to explain this. Mode coupling theory explained their experimental findings very well.

They used the Minkowski measures approach to describe the topographies that emerged in simulations and experiments on dewetting liquid films. The experimental and simulated patterns strongly resembled each other, so numerical simulation can be used to test the behaviour of a liquid on a hypothetical substrate and to predict stability conditions.

Future studies will concentrate on the energy dissipation close to the three-phase contact line of a moving front, addressing questions like: Can the front profile be used to describe a liquid's properties? Does it reveal whether the liquid is sliding over the surface? Do liquids containing particles or blends of liquids behave similarly? Can we enhance the throughput of lab-on-a-chip devices?

Chirality of nanotubes

Nondispersive and dispersive collective electronic modes in carbon nanotubes
Ricardo Perez and William Que
J. Phys.: Condens. Matter
17 (2005) L367–L372

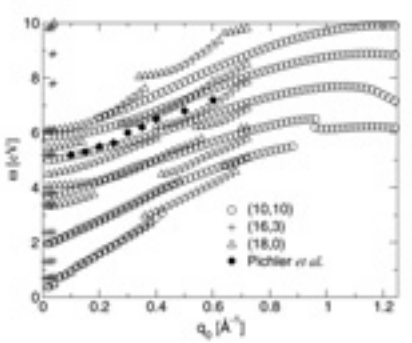

Dispersion curves for the collective electronic modes with angular momentum index $L = 0$, for three carbon nanotubes. The solid diamonds are experimental results on the dispersive mode from Pichler et al. The Brillouin zone edges for the (10, 10), (18, 0), and (16, 3) carbon nanotubes are at $q_0 = 1.26$, 0.73, and 0.041 Å^{-1}, respectively.

Metallic carbon nanotubes show Luttinger liquid behaviour, by which single-particle excitations are suppressed and collective electronic modes or plasmons play an important role. Momentum-dependent EELS experiments on single-wall carbon nanotubes carried out by Pichler *et al* in 1998 showed a dispersive mode attributed to the π plasmon and several non dispersive modes at lower energies whose origin is controversial: at least three different interpretations have been offered, but none of these was consistent with new results from optical absorption measurements

Ricardo Perez and William Que of Ryerson University, Canada, present their theoretical results on the loss functions of individual single-wall carbon nanotubes and shed some light on the origin of the non dispersive modes, which they propose are inter(sub)band plasmons from chiral nanotubes with small Brillouin zones.

They use such a tight-binding model for π band electrons to study the collective electronic excitations of individual nanotubes using the random phase approximation. The calculated dispersion curves of collective electronic modes for $L = 0$ are shown in the figure. The dispersion curves terminate at the Brillouin zone edge of the corresponding nanotube. We see that the (16, 3) tube has only optical modes, while the (10, 10) and (18, 0) tubes each have an acoustic mode. This is because the (16, 3) tube is semiconducting while the other tubes are metallic.

Note that, since the experiment of Pichler *et al* was performed on bulk samples, the measured spectra contain contributions from many nanotubes of different chirality. The non dispersive modes could be due to chiral nanotubes, and the dispersive mode should be due to armchair and zigzag nanotubes. Since intertube coupling shifts the energies of the collective electronic modes higher, it is not possible to match the calculated energies in this work for individual nanotubes to experimental results on bulk samples where intertube coupling is present. To allow an exact comparison between theory and experiment, it is desirable to obtain momentum-dependent EELS for individual nanotubes, and such experiments should determine the validity of the interpretation offered here. If Perez and Que's prediction is confirmed experimentally, eventually EELS could become a potential tool for identifying the chirality of individual carbon nanotubes.

Five-wave mixing at surfaces

Femtosecond time-resolved five-wave mixing at silicon surfaces
T Meier, M Reichelt, S W Koch and U Höfer
J. Phys.: Condens. Matter
17 (2005) S221–S244

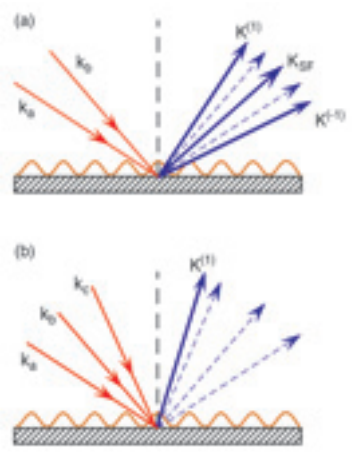

A schematic drawing of wave-mixing processes at surfaces in reflection geometry; (a) for two and (b) for three incident laser beams.

Two-photon photoemission (2PPE) measurements are generally restricted to conducting surfaces. T Meier, M Reichelt, SW Koch and U Höfer describe a surface-sensitive time-resolved technique combining four-wave mixing (4WM) with second-harmonic generation (SHG), resulting in a five-wave-mixing (5WM) process and review recent experimental results on silicon surfaces. The diffracted second harmonic generated by sequences of ultrashort laser pulses is detected as a function of the time delay between the pulses. This 5WM technique can be used to measure the temporal evolution of the optical polarization and the photoexcited populations at the surface.

At the Si(111)7 × 7 surface, the self-diffracted signal induced by two ultrashort laser beams shows a rapid decay on a timescale comparable with the duration of the incident pulses of less than 15 fs. Numerical solutions of the optical Bloch equations for model systems show that it cannot be decided from the experimental data alone whether this dynamics is due to the decay of individual uncoupled polarizations or is the result of the destructive interference of a system of coupled polarizations. To distinguish these processes, a microscopic modelling of the SHG including all optical matrix elements and further relevant interaction processes is required.

The Si(001)c(4 × 2) surface has been studied using a 5WM set-up which measures the diffracted second-harmonic intensity induced by three femtosecond laser beams. By varying individual time delays between the pulses, this technique can be used to investigate the dynamics of one-photon transitions, and also allows one to monitor the temporal evolution of populations. Using model calculations based on optical Bloch equations, the observed ultrafast response as a function of a particular delay can be assigned to scattering of the excited electrons within the D_{down} surface band on timescales of 50–500 fs.

The authors plan similar 5WM experiments using tunable laser pulses to investigate these processes in more detail, analyse the ultrafast optically induced dynamics at other surfaces, and access the largely unexplored electron dynamics of buried semiconductor interfaces. Theoretically, more microscopic approaches will be developed to gain a better quantitative understanding of the material dynamics responsible for the dynamics of nonlinear optical excitations at surfaces and interfaces.

Molecular motor

Biasing the random walk of a molecular motor
R Dean Astumian
J. Phys.: Condens. Matter
17 (2005) S3753–S3766

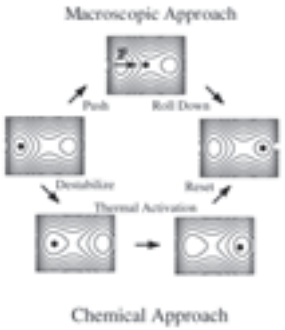

Cartoon illustration of the difference between a mechanical and a chemical approach for storing energy by transferring a particle from a low energy well to a well at a higher energy. Because of the 'softness' of the potential, in the 'macroscopic approach' an external source provides a force to push the molecule over the barrier. Side to side motion due to thermal noise would result in a longer path to the top, and thus require more energy from the external source than the minimum, $E_A^{\ddagger}$, resulting in an inefficient motor. In the chemical approach however the input energy is used to destabilize the system in the left-hand well, but the motion itself is driven by thermal activation over the barrier. In this case, the side to side jitter does not decrease the efficiency.

Biomolecular motors are molecules that convert chemical free energy into directed motion. Rather than talking about levers, springs and dashpots, judo throws, rowing cross-bridges, or power strokes, molecular motors should be discussed in terms of equilibrium processes.

The sequence of conformational changes by which a motor protein moves is a random walk, with transitions occurring by thermal activation over energy barriers. Dean Astumian of University of Maine addresses the question of how this random walk is biased by a non-equilibrium chemical reaction (ATP hydrolysis) so the motor molecule moves preferentially in one direction and discusses how these 'soft matter' motors can achieve thermodynamic efficiencies of nearly 100%.

The motions of molecular motors are best described as thermally activated stochastic processes with Poisson distributed lifetimes. The Brownian motor mechanism is based on thermally activated transitions between states that are very close to 'local' equilibrium with respect to their internal degrees of freedom despite the fact that the chemical reaction that drives motion, ATP hydrolysis, is very far from equilibrium. By operating where all conformational states are near to local equilibrium and by using a chemical (stabilization/destabilization) approach rather than a mechanical approach, a biomolecular motor made of 'soft', conformationally flexible, protein can operate at nearly perfect efficiency.

Soon the mechanism of biomolecular motors will be clarified experimentally. By observing at a single-molecule level an individual ATP hydrolysis event followed by the completion of a step of the motor along its track, the distribution of time lapse between these two events can be determined. The random walk (Brownian motor) model presented here predicts that the time between ATP hydrolysis and completion of a step will be randomly (Poisson) distributed rather than deterministic as expected from a mechanical model. Resolution of this question will be important not only for understanding the mechanisms of biomolecular motors, but also in the design of synthetic molecular motors.

Magnetoelectronics with magnetoelectrics

Magnetoelectronics with magnetoelectrics
Ch Binek and B Doudin
J. Phys.: Condens. Matter
17 (2005) L39–L44

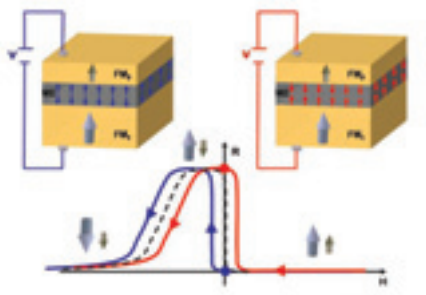

Schematics of the magnetoresistance curve of a TMR device involving an ME film as a tunnel barrier. Half-hysteresis curves are shown, after saturation at positive field values. The arrows denote the magnetization directions, with the bottom layer FM1 being harder (or pinned) than the top one FM2. The dashed curve is the expected TMR behaviour. The change of voltage polarity changes the direction of the net magnetization of the ME layer, adding an exchange bias magnetic field to the resistance curve. The two colours indicate shifting of half-hysteresis curves towards positive or negative fields, depending on the polarity of the applied voltage. At zero magnetic field, the change of voltage polarity changes the resistance value of the device (dots).

Applications of spintronics such as magnetic read-heads and sensors use giant magnetoresistance (GMR) and tunnel magnetoresistance (TMR) effects. The next generation of spintronics devices should combine memory and logical functions.

Ch Binek and B Doudin from University of Nebraska propose combining a GMR or TMR device with a magnetoelectric (ME) film. They propose an antiferromagnetic ME thin film as a dielectric tunnel junction between two ferromagnetic metallic layers. A tunnel barrier is the ideal system for sustaining very high electric fields, so they expect a significant net magnetization to occur in an ME barrier. The device exploits the exchange field between the magnetized ME layer and the two adjacent ferromagnetic films. This creates a shift of the magnetization curves of both ferromagnetic layers proportional to the magnetization in the ME layer, or the applied voltage in the device. The figure shows a TMR device made of a soft magnetic layer FM2 and a hard bottom layer FM1. An exchange field value of the order of the saturation field of the soft magnetic layer will provide control of the magnetization direction of the soft layer, allowing the resistance state of the device to be set by the electric field in the ME film. They also proposed a similar device based on spin valves used in GMR systems.

Pure electrical control of magnetic configurations of giant magnetoresistance spin valves and tunnelling magnetoresistance elements is achievable. Estimates based on documented ME tensor values show that exchange fields reaching 100 mT can be obtained. They propose a mechanism alternative to current-induced magnetization switching, providing access to a wide range of device impedance values and opening the possibility of simple logic functions.

Muonium observations of SiGe alloys

Characterization of hydrogen-like states in bulk $Si_{1-x}Ge_x$ alloys through muonium observations
P J C King, R L Lichti, S P Cottrell, I Yonenaga and B Hitti
J. Phys.: Condens. Matter
17 (2005) 4567–4578

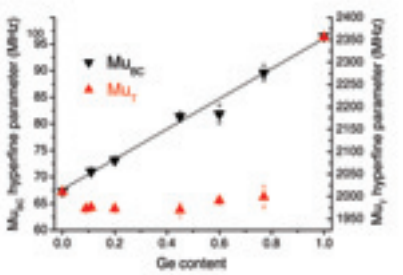

Variation with alloy composition of the average value of the isotropic component of the Mu_{BC} HP, with straight line fit, together with the Mu_T HP

Hydrogen is a common impurity in semiconductors but its study can be difficult because of its high reactivity. The light hydrogen-like atom muonium, formed of a positive muon and an electron, is electronically almost identical to hydrogen, and so provides a good guide to its electronic states.

In silicon and germanium two muonium states are formed at low temperatures: an immobile, bond-centred species Mu_{BC}, and a rapidly-diffusing tetrahedral-site centre Mu_T.

P J C King at Rutherford Appleton Laboratory and co-workers at Texas Tech University, Tohoku University, and TRIUMF, Vancouver, have measured the Mu_T and Mu_{BC} hyperfine parameters (HP) in bulk $Si_{1-x}Ge_x$ alloy by implantation of spin-polarized, positive muons, and observation of the muon polarization inside the sample through detection of the positrons emitted when the muons decay.

The figure shows the observed linear variation of the isotropic component of the Mu_{BC} HP with x. Within bulk $Si_{1-x}Ge_x$ alloys there is a random site occupancy of Ge and Si atoms. Also, the Ge–Ge, Ge–Si and Si–Si bond lengths are different and vary linearly with alloy composition. Implanted muons adopting an immobile, bond-centred position therefore experience a random selection of bonding environments which overall show a linear variation with alloy composition.

The figure also shows the very non-linear behaviour of the Mu_T HP with x. The T-site to T-site hop rate of the Mu atom is much faster in Ge than in Si. The expected path between adjacent T-sites is through the centre of the puckered six-member ring separating adjacent tetrahedral cages, which is larger in Ge than in Si. Further, the electronic charge distribution and the overall energy landscape within which a Mu atom moves are considerably flatter for Ge than for Si.

The temperature dependence of the Mu_T HP in $Si_{1-x}Ge_x$ alloys is more complex than has been previously suggested for pure Si, and suggests it is governed by interaction with phonon modes in a more involved way than has been described by previous models. A more complete model is needed to provide an accurate description.

Heavy fermions

Dynamics and transport properties of heavy fermions: theory
Optical and transport properties of heavy fermions: theory compared to experiment
David E Logan and N S Vidhyadhiraja
J. Phys.: Condens. Matter
17 (2005) 2935–2958 and 2959–2976

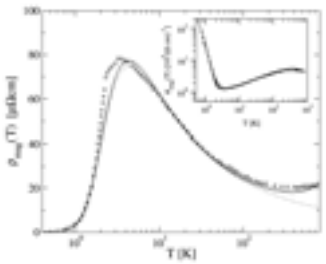

Comparison of experimental $\rho^{exp}_{mag}(T)$ for CeB_6 with theory, on a log–linear scale. Inset: the dc conductivity $\sigma^{mag}(T) \equiv 1/\rho_{mag}(T)$ on a log–log scale

Heavy electron materials have been extensively investigated, yet even their 'normal' paramagnetic phase, be it metallic or insulating, has eluded a unified microscopic description on all temperature (T) and/or frequency (ω) scales. Within the general framework of dynamical mean-field theory David Logan and N S Vidhyadhiraja (Oxford) have developed a non-perturbative local moment approach to paramagnetic metallic phases of the periodic Anderson model (PAM), with a focus on dc transport and optics, focusing on the Kondo lattice regime relevant to strong correlated heavy fermion (HF) metals, where the problem is characterized by a single, exponentially small coherence scale ω_L. All relevant energy/temperature scales are handled by the theory, from the low-energy coherent Fermi liquid domain out to large multiples of ω_L where incoherent many-body scattering dominates; followed by the crossover out of the scaling regime to non-universal, high-energy/temperature scales dictated by 'bare' model/material parameters. While the emphasis has been on strong correlations, all interaction strengths are encompassed by the LMA, so intermediate valence behaviour can also be addressed.

In the second paper they make a direct comparison with the dc transport and optical conductivities of CeB_6, $YbAl_3$, $CeAl_3$ and $CeCoIn_5$. $YbAl_3$ is an intermediate valence material, and the others typify heavy fermion behaviour, from the strongly correlated Kondo lattice regime of $CeAl_3$ and CeB_6 to the somewhat weaker coupling case of $CeCoIn_5$. Most features of the optics and transport of these materials are captured, the natural exception, omitted from the model itself, being crystal field effects which may (or may not) show up in the experimental resistivity as a reduction below one-channel behaviour at suitably high temperatures. The theory performs well quantitatively, and also captures notable features specific to individual systems, e.g. the existence of a low-frequency shoulder in the optics of $YbAl_3$, or the absence of any significant direct gap/mIR absorption in $CeAl_3$. The model thus appears to provide quite a comprehensive and successful description of experiment. This the authors attribute both to the dominance of the local electron scattering inherent to the model itself and the need to provide an adequate theoretical description of such on all experimentally relevant frequency and temperature scales.

Novel superconductivity in $CePt_3Si$

Novel superconductivity coexisting with incipient electric-multipolar order in $CePt_3Si$

M Ishikawa, S Yamashita, Y Nakazawa, N Wada and N Takeda

J. Phys.: Condens. Matter
17 (2005) L231–L234

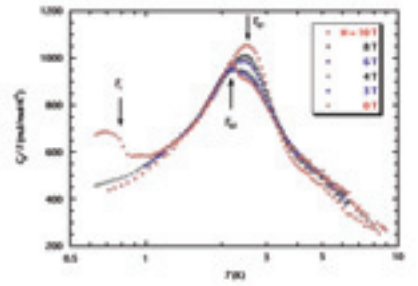

C_p/T versus ln T as a function of several magnetic fields for an annealed sample of $CePt_3Si$. T_{Q1}, T_{Q2} and T_c are respectively two quadrupolar-like transitions and superconducting transition temperature.

There is much interest in strongly correlated electron systems, e.g. the unconventional superconductivity in f-electron heavy-fermion compounds including $CePd_2Si_2$, $CeIn_3$, $CeRh_2Si_2$, $CeCu_2Si_2$, UPt_3 and $CePt_3Si$. Pairings mediated by fluctuations of spin, valence, density have been proposed. $CePt_3Si$ is claimed as a new superconductor without inversion symmetry, and its pairing mechanism is actively sought.

M Ishikawa and co-workers in Japan recently reported that an annealed sample of $CePt_3Si$ exhibits non-magnetic heavy-fermion behaviour. To reveal the precise nature of the 2.2 K transition, they measured Cp above 0.6 K in fields up to 10 T. The plot of Cp/T versus ln T shows a small but distinct anomaly at 2.2 K and a shoulder around 2.8 K at zero field, denoted T_{Q2} and T_{Q1}, respectively. The former is rapidly depressed and absorbed by the latter below about 4 T, and the latter becomes sharper and grows into a distinct peak as the field increases. This resembles the quadrupolar transitions in CeB_6 and $Ce_3Pd_{20}Ge_6$. The transition at T_{Q1} may be an incipient quadrupolar transition. However, in CeB_6 an AF transition occurs at 2.5 K in the quadrupolar-ordered phase, while the present transition at T_{Q2} is not AF but something related to the transition at T_{Q1}. Superconductivity emerges below these temperatures but is destroyed by a field around 4 T as the T_{Q2} peak is smeared out. The new phase at T_{Q2} may assist the appearance of superconductivity.

Why is such coexistence feasible in $CePt_3Si$? The heavy-fermion state with relatively large exchange interaction parameter $\mathcal{J}_{cf}$ is formed closer to an intermediate-valence region rather than a quantum critical point on the verge of an AF phase. A large $\mathcal{J}_{cf}$ and high Kondo temperature are inferred from the exceedingly low magnetic entropy at these low temperatures. I.e., it is in a state where strong fluctuations of any kind are conceivable near the presumed multipolar transition, and the superconductivity could be mediated via such fluctuations of spin, valence or charge, as proposed for superconductivity in other heavy-fermion compounds like $CePd_2Si_2$ and $CeCu_2Si_2$. It is important to decide which type of fluctuation is most effective for the superconductivity in $CePt_3Si$.

Short-range attractions in proteins

Tuning short-range attractions in protein solutions: from attractive glasses to equilibrium clusters

Anna Stradner, George M Thurston and Peter Schurtenberger

J. Phys.: Condens. Matter
17 (2005) S2805–S2816

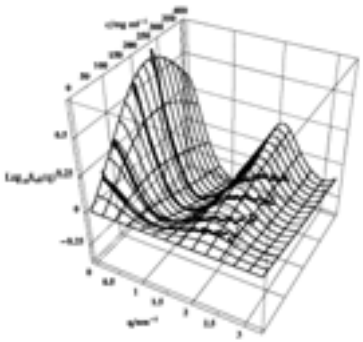

Effective structure factors $S_{eff}(q)$ for γ B-crystallin solutions plotted vertically as a function of q and protein concentration c, compared with the Baxter sticky sphere structure factor model with use of sphere diameter 3.6 nm and stickiness parameter $1/\tau = 8.62$

Anna Stradner and Peter Schurtenberger of Fribourg University, Switzerland, and George Thurston of Rochester Institute of Technology, USA have carried out small-angle scattering experiments with two different types of model proteins, γ B-crystallin and lysozyme.

They discuss the results in the context of recent suggestions that globular proteins possess a short-ranged attractive potential, and that simple models from colloid science could help to rationalize the best route for obtaining protein crystals and to interpret their complex phase diagrams. The short-range attraction leads to an extremely interesting phase behaviour with a liquid–gas coexistence curve that is metastable with respect to the liquid–solid (crystal) boundary and the occurrence of an attractive glass. They demonstrate that for γ B-crystallin, the scattering data are indeed in good agreement with predictions for an interaction potential consisting of short-ranged attraction and hard sphere repulsion, and they also provide evidence of a dynamically arrested glass or gel phase at high concentrations. They also report on a systematic study of the effect of a weak screened Coulomb repulsion in highly concentrated lysozyme solutions.

They have previously shown that a combination of short-range attraction and long-range repulsion results in the formation of small equilibrium clusters, which is clearly relevant for e.g. nucleation processes during protein crystallization, protein or DNA self-assembly, and the formation of cluster and gel phases in colloidal suspensions. In the current study they investigate the effect of variations in temperature, which allows them to carefully tune the balance between soft repulsion and short-range attraction and investigate its influence on the cluster formation.

Any attempt to use the theoretical framework for strongly interacting colloidal particles, e.g. to use mode-coupling theory to evaluate particle dynamics close to dynamical arrest near a glass or gel line, requires precise knowledge of the static structure factor $S(q)$, so they used a combination of small-angle x-ray and neutron scattering to determine $S(q)$ as a function of concentration, ionic strength and temperature for both lysozyme and γ B-crystallin. This provides structural information on the spatial correlations between individual proteins in concentrated solutions.

s–p- and d-ferromagnetism

Are s–p- and d-ferromagnetisms of the same origin?

Antonis N Andriotis, R Michael Sheetz and Madhu Menon

J. Phys.: Condens. Matter
17 (2005) L35–L38

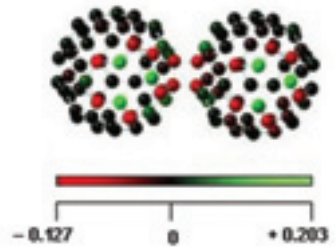

Figure showing the effect of charge transfer induced by the vacancy and the presence of 2 + 2 cycloaddition. The atoms surrounding the vacancy are positively charged while the atoms participating in the cycloaddition are negatively charged.

There is much current interest in the exotic s–p magnetism in organic materials such as C_{60}-based polymers and some non-traditional inorganic materials such as hexaborides. These materials show several common features, such as the presence of structural and/or topological defects, significant charge transfer, a degenerate ground state and, in some cases, a resonant ground state.

Antonis N Andriotis of FORTH and R Michael Sheetz and Madhu Menon of University of Kentucky have examined the results in more detail, emphasizing the defect-related magnetism in the C_{60}-based polymers and elucidated the underlying mechanism of their magnetism. They draw analogies with the well known McConnell model for ferromagnetic charge-transfer salts.

The existence of the 2 + 2 cycloaddition bonds (which provide sp_3-bonded carbon atoms) in coexistence with vacancies can explain the magnetism in polymerized-C_{60} materials. The vacancies and the 2 + 2 cycloaddition bonds provide the necessary unpaired electrons, while also initiating the charge-transfer processes which create and sustain large electric dipole moments. The latter develop the necessary ferromagnetic coupling mechanism among the unpaired spins, leading to a ferromagnetic state.

These observations show the common origin and common features of s–p magnetism and the usual d-magnetism. Charge-transfer processes and orbital degeneracy seem to be key factors. However, the charge-transfer processes have to be large enough to develop and sustain strong fields to provide the necessary kinetic exchange interaction for promoting the high spin states as ground states, and this is more apparent in s–p magnetism. The differentiation between the two types of magnetism in the literature through various models reflects the leading terms that are kept in the implementation of the e–e correlations and the underlying physical picture of such an approximation.

Shape-memory effect

Fermi surface as a driver for the shape-memory effect in AuZn

R D McDonald, J Singleton, P A Goddard, F Drymiotis, N Harrison, H Harima, M-T Suzuki, A Saxena, T Darling, A Migliori, J L Smith and J C Lashley

J. Phys.: Condens. Matter
17 (2005) L69–L75

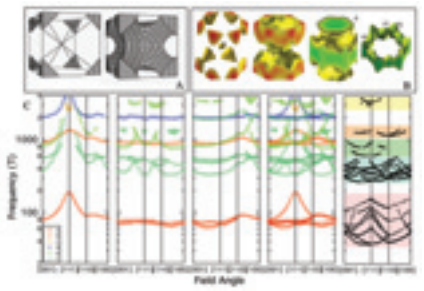

The calculated Fermi surfaces for (A) the austenite phase and (B) martensite phase of AuZn; the small letters label the orbits giving rise to various dHvA oscillations. (C) (from left to right) dHvA frequencies from the band-structure calculations for the martensite domain with the c-axis oriented along the austenite [111] direction, the [11̄1] and [1̄11] directions and the [1̄1̄1] direction and the sum of all domain orientations, with the observed dHvA frequencies on the right. The coloured bands are a guide to the eye, a–f indicate the Fermi-surface orbits responsible for each frequency (see (B)).

Martensites are widely found materials that undergo diffusionless, solid-state transitions. Some of them exhibit the shape-memory effect (SME) - after deformation of the low-temperature martensitic phase, they recover their high-temperature shape on warming.

A group let by John Singleton (Los Alamos) has identified the primary electronic mechanism responsible for the martensitic transition (MT) in the shape-memory alloy AuZn through detailed measurements of its Fermi surface and comparing the data with band-structure calculations.

As the temperature is lowered through the MT, the unit cell is distorted in the [110] shear direction. A strain and commensurate shuffle of every third unit cell results in a hexagonal primitive unit cell formed from nine primitive cubic cells of the parent phase.

The figure shows the calculated Fermi-surface sections of the martensite phase (B) along with their predicted de Haas–van Alphen (dHvA) frequencies as a function of field orientation (C). There is good agreement between the experimental and theoretical frequencies.

Magnetoresistance data show that the MT in AuZn is associated with a single, distinct rearrangement of the Fermi surface. Together with heat capacity experiments, this shows that the MT is free of the complications of precursor phases. Furthermore, the low transition temperatures rule out effects due to diffusion and vibrational entropy. The dHvA data suggest an order-of-magnitude length scale for the martensite domains and agree with band structure calculations. The data and calculations provide direct evidence about the role of the band-electron system and its Fermi surface in the SME, showing that band-structure/property relations are an important consideration for the design of future SME alloys.

Chirality and protein folding

Chirality and protein folding

Joanna I Kwiecińska and Marek Cieplak

J. Phys.: Condens. Matter
17 (2005) S1565–S1580

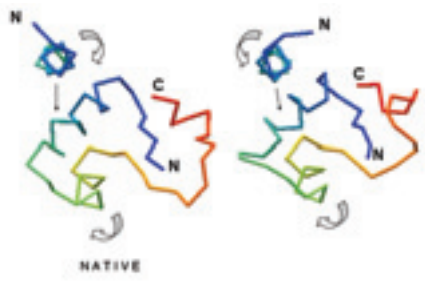

Conformations of crambin in the backbone representation. Left: the native structure (1crn in the Protein Data Bank). Right: the conformation in which all native contacts are established through a folding process accomplished through a molecular dynamics evolution in the Go-like model. Some local chiralities are opposite to what they should be.

A problem in modelling the kinetics of protein folding is to know when the system has reached the native conformation. Simple and widely used criteria of folding are based on a variable crossing a predefined threshold value, rc , e.g. the root mean square deviation (RMSD) distance away from the native state, or the fraction, Q, of the established native contacts. A third criterion, based on the angular properties of the protein backbone, involves checking whether the bond and dihedral angles are within a chosen range of their native values.

Joanna Kwiecińska and Marek Cieplak of Polish Academy of Sciences, Warsaw show that such simple criteria may prompt one to declare folding even though fragments of the resulting conformations have the wrong chirality. The figure shows an example of this with the Q criterion. The folding process may generate a left-handed α-helix instead of the true right-handed one, even though all native contacts are within their respective values of r_c and the RMSD distance from the native state is only around 2.5 Å.

They propose combining the simple criteria with the requirement that all local values of the chirality should be nearly native. They show that setting the local chiralities to native-like values may or may not precede the 'calls' resulting from the simple criteria, but the compound requirement allows for more accurate studies of folding and typically generates structures that appear to be of correct topology.

They discuss the questions of how the chirality-based criterion relates to the criterion involving the bond and dihedral angles and whether it is better to use potentials that favour the native sense of chirality or those which favour the native values of the bond and dihedral angles. They find the chirality potential to act in a comparable way to the angular potential, but its usage is much more economical in simulations. They also find that simple modelling of the side groups by the β carbon atoms does not automatically make the chirality in the folded state correct.

Magnetotransport in $Zn_{1-x}Co_xO$ films

Magnetotransport in epitaxial films of the degenerate semiconductor $Zn_{1-x}Co_xO$

R C Budhani, Prita Pant, R K Rakshit, K Senapati, S Mandal, N K Pandey and Jitendra Kumar

J. Phys.: Condens. Matter 17 (2005) 75–86

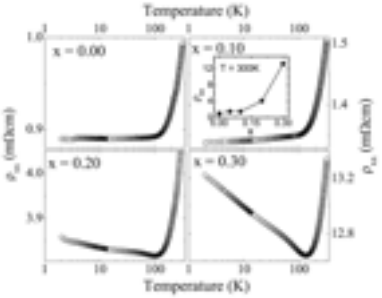

The zero-field longitudinal resistivity of the films with x = 0.0, 0.10, 0.20 and 0.30 plotted as a function of temperature. The inset shows the variation of the room temperature resistivity as a function of the cobalt concentration.

ZnO doped with transition metal (TM) is a strong candidate for a dilute magnetic semiconductor (DMS). The origin of the long-range ferromagnetic order observed well above 300 K is controversial. In some cases the magnetism was related to isolated clusters of the TM or its oxides, whereas in others a seemingly homogeneous solid solution orders via alignment of 3d spins at the TM ion sites.

The solubility of Co is larger in thin films than in bulk samples, but there are conflicting reports on the magnetic character of these films. R C Budhani and co-workers at Indian Institute of Technology, Kanpur have performed magnetotransport measurements over a broad range of temperatures and magnetic fields on highly degenerate n-type $Zn_{1-x}Co_xO$ epitaxial films. The cobalt-free samples are characterized by a metallic resistivity $\rho(T)$ down to 2 K, a negative and predominantly isotropic magnetoresistance and optical transmission above 85% in the visible range. X-ray diffraction measurements showed that, while for $x < 0.20$ all cobalt atoms occupy the tetrahedral sites of the wurtzite structure of ZnO, a phase separation into CoO is seen for $x > 0.2$. In the solution phase, they did not observe any signatures of a spontaneous ordering of the cobalt spins despite a large concentration of mobile electrons ($>10^{20}$ cm^{-3}). The absence of anomalous Hall resistance is consistent with this observation. Over the entire range of x, the carrier concentration remains above the Mott limit for the insulator-to-metal transition in a doped semiconductor. However, while the Co-free samples are metallic ($T > 2$ K), there is a resistivity minimum followed by ln T divergence of $\rho(T)$ at low temperatures with increasing x. The magnetoresistance of these samples is negative and predominantly isotropic and tends to follow a log H behaviour at high fields. These observations, including the Kondo-like minimum in the resistivity, suggest transport in these dilute magnetic semiconductors is dominated by s–d exchange.

Hydrogen production from ethanol on Pt(111)

Modelling of ethanol decomposition on Pt(111): a comparison with experiment and density functional theory

E Vesselli, G Coslovich, G Comelli and R Rosei

J. Phys.: Condens. Matter
17 (2005) 6139–6148

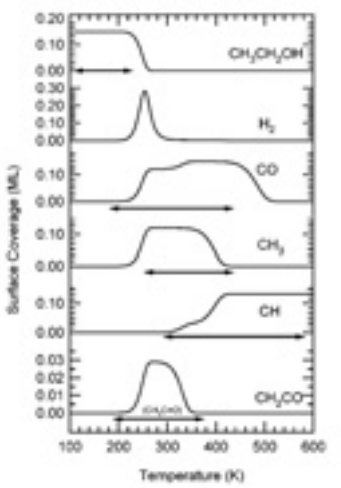

Surface concentration of the stable species during a simulated ethanol decomposition experiment on Pt(111), as a function of temperature, on the basis of the results obtained with the simple UBI-QEP model. Arrows indicate the temperature range in which the species are found to be stable on the basis of real time temperature-dependent XPS data

The ethanol reforming reaction catalysed by Pt or Rh is a candidate for hydrogen production. E Vesselli and co-workers in Trieste have studied ethanol decomposition on clean Pt(111) in the zero-coverage limit in the unity bond index-quadratic exponent potential (UBI-QEP) model.

DFT identifies ethanol, CH_3CHOH, CH_3COH, CH_3CO, CH_2CO, CHCO and CCO as the most stable intermediates for each dehydrogenation step from ethanol to CCO. CH_3COH has the lowest transition state energy for C-O cleavage, while CHCO shows the lowest decarbonylation barrier. These results predict that C-C cleavage is faster than C-O dissociation on Pt(111) above 550 K.

UHV experiments have shown that ethanol adsorbs molecularly at 100 K on Pt(111). The decomposition reaction at higher temperature proceeds via a metastable intermediate (CH_3CO?), which forms CO and CH or CH_3 groups via C-C bond cleavage. It is proposed that CH_3CO dehydrogenates to CHCO (unstable), yielding CO and CH, which rehydrogenates to methane.

Vesselli *et al* used the UBI-QEP model to simulate the most probable decomposition pathway. They found good estimates for adsorption energies and dehydrogenation barriers but their C-C and C-O bond cleavage barriers (though in line with experiment) disagreed with DFT estimates. Their kinetic picture can explain these discrepancies. The proposed reaction mechanism predicts the formation of CH_3 and CH groups on the surface by distinct parallel reaction paths. Then, the methyl groups can rehydrogenate to methane or dissociate to surface carbon and hydrogen. The proposed stable intermediate is CH_2CO, which is not incompatible with the spectroscopic data. This work is a further step in predicting catalytic behaviour.

Dynamics of active filaments

Some aspects of the dynamics of active filament solutions

Tanniemola B Liverpool

J. Phys.: Condens. Matter
17 (2005) S1153–S1163

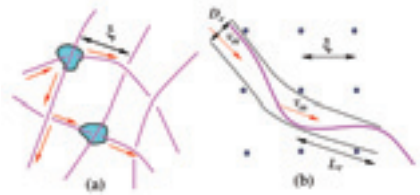

(a) The active solution with motor centres and entanglement points. (b) The 'tube' encircling the polymer and the directed motion v_m.

Soft active systems are a new and exciting class of complex fluids to which energy is continuously supplied by internal or external sources. Examples from biology include cell membranes and biopolymer solutions driven by chemical reactions, living cells moving on a substrate, and the cytoskeleton of eukariotic cells. The cytoskeleton is a complex network of long filamentary proteins cross-linked by smaller proteins. Among the latter are clusters of motor proteins, such as myosin and kinesin, that use chemical energy from the hydrolysis of ATP to 'walk' along the filaments. This out-of-equilibrium chemical activity in motor–filament solutions leads to complex cooperative behaviour including pattern formation and creation of dissipative structures.

Tanniemola Liverpool of Leeds University has studied certain aspects of these motor–filament systems. First he considers the linear viscoelastic response of an isotropic solution of entangled polar filaments interacting with motor clusters in the regime where the motors do not lead to the formation of macroscopic patterns. Next, using a hydrodynamic approach, he investigates the stability of the isotropic state to the formation of ordered states or patterns. Finally he discusses a microscopic model of the filament–motor interaction enabling the parameters of the hydrodynamic model to be derived.

The rich behaviour of mixtures of filaments and motors is far from being completely understood. The simple picture considered needs to be tested by experiment. Even in the isotropic regime, an active solution could be pre-stressed, and it is possible that imposing a shear flow could decrease the stress. It is assumed that the tube has the same properties as those of a passive solution, while it is reasonable to expect its properties to be changed by activity. The assumption that the active fluctuations couple only to the longitudinal modes also needs to be tested.

More work is needed to understand the nature of the spatially inhomogeneous state. Motor transport was not included in the above description, but it is important for very processive motors and at low motor densities. The effect of shear flow on the formation and stability of spatially inhomogeneous structures should also be studied.

Liquid–liquid phase transitions

On the abundance and general nature of the liquid–liquid phase transition in molecular systems

Rei Kurita and Hajime Tanaka

J. Phys.: Condens. Matter
17 (2005) L293–L302

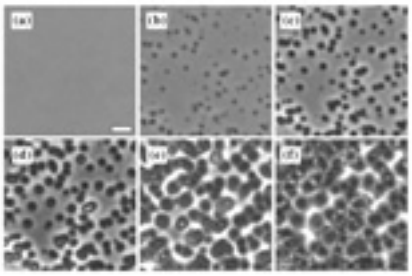

Patterns observed with phase contrast microscopy at T_a = 120 K for various annealing times t_a: (a) 30 min, (b) 45 min, (c) 60 min, (d) 90 min, (e) 120 min, and (f) 180 min. The scale bar corresponds to 20 μm. Initially there is only liquid I (see (a)), and then droplets of liquid II with dark contrast appear and grow with time.

Even a single-component liquid may have more than two kinds of isotropic liquid state. Although there are clear examples of liquid–liquid transitions (LLT) for atomic liquids, there was until recently no direct evidence for molecular liquids. LLT in water has been suggested by experimental evidence of polyamorphism and numerical simulations. Recently, Hajime Tanaka and colleagues from the University of Tokyo found convincing experimental evidence of LLT in a molecular liquid, triphenyl phosphite (TPP). Both nucleation-growth-type and spinodal-decomposition-type phase transformations were directly observed with optical microscopy. The glass transition of a normal liquid and a distinct thermal signature of the glass transition of a second liquid were both detected. They also observed a critical-like anomaly associated with the mean-field spinodal behaviour of LLT.

Tanaka *et al* have now reported another example of LLT in a molecular liquid, n-butanol using phase-contrast microscopy. The figure shows the pattern evolution process observed when n-butanol was quenched at 5 K min^{-1} and annealed at 120 K, where it is a supercooled liquid. These data suggest that liquid I eventually transforms into homogeneous liquid II.

TPP and n-butanol have quite different molecular structure, but show very similar LLT behaviour, so LLT may be common in molecular liquids. As LLT is insensitive to the details of molecular or chemical structures, its only requirement may be the cooperative formation of locally favoured structures, whose type depends on the molecular structure, but cooperative short-range bond ordering may be universal. For TPP and n-butanol, for example, hydrogen bonding may be crucial in the formation of such structures. The identification of the locally favoured structures of these liquids remains a future problem.

This study may shed new light on the basic nature of a liquid: even an ordinary molecular liquid such as n-butanol or TPP may have a hierarchical energetic structure, being neither perfectly homogeneous nor random, but possessing long-lived short-range order with cooperativity. So, the liquid may not be a unique state of matter, but there can often be more than two liquid states even for single-component matter. LLT may be hidden by either crystallization or glass transition. The former may be the case of liquid water.

Slow dynamics

Slow dynamics in glassy soft matter
Luca Cipelletti and Laurence Ramos
J. Phys.: Condens. Matter
17 (2005) R253–R285

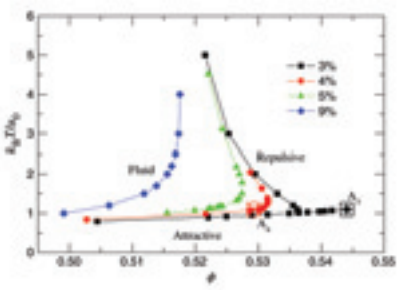

Theoretical phase diagram for hard spheres of radius R with a square well attractive interaction of width > and depth u_0. Curves are labelled by the relative well width, ξ= /(2R+). Note the re-entrant shape of the lines separating the fluid region to the glassy regions for ξ < 5%. For ξ = 3% a line separating the attractive and the repulsive glass phases ends in the A_3 singular point. The A_4 singular point (circled cross) is estimated to be located on the ξ = 4.11% line (not shown for clarity).

Luca Cipelletti and Laurence Ramos from Montpellier review recent experimental work on the slow dynamics in soft matter, focusing on four closely related areas: the existence of two different glass states (attractive and repulsive), the dynamics and the ageing of systems far from equilibrium, the effect of an external perturbation on glassy materials, and dynamical heterogeneity.

Many unified approaches have been sought to account for the similarities in the slow dynamics of many soft materials and analogies with hard condensed matter glasses and granular media, notably mode coupling theory (MCT). Recent theoretical work shows that MCT can make quantitative predictions on dynamical heterogeneity: they need to be tested experimentally.

The jamming scenario can rationalize fluid-to-solid transitions in systems ranging from colloidal suspensions to molecular glasses and granular materials. It is supported by analogies in the local dynamics between glass formers and granular media (cage effect, dynamical heterogeneity).

While MCT and jamming describe systems approaching the non-ergodicity transition from the fluid phase, materials deeply quenched in an out-of-equilibrium phase are less well understood. The effective temperature concept may prove useful to describe out-of-equilibrium soft materials and their ageing, but experimental values are contradictory. Stress relaxation appears to be important in the slow dynamics of many soft glasses, though it has been generally neglected in theoretical approaches.

Slow dynamics in glassy soft matter has been investigated by a combination of theory, simulation, and experiments. New experimental techniques have extended measurements to out-of-equilibrium and very slowly relaxing systems, aiming to obtain spatially and time-resolved information on the dynamics, and to identify the most insightful quantities to characterize heterogeneous behaviour. Future advances will probably include the combined use of these methods, to achieve a more complete understanding of the various physical mechanisms driving the relaxation of glassy soft matter, and of their interplay. The focus will be in identifying and explaining the 'universal' features of the slow dynamics in vastly different systems.

Flow-induced structures in colloids

Flow-induced structure in colloidal suspensions
J Vermant and M J Solomon
J. Phys.: Condens. Matter
17 (2005) R187–R216

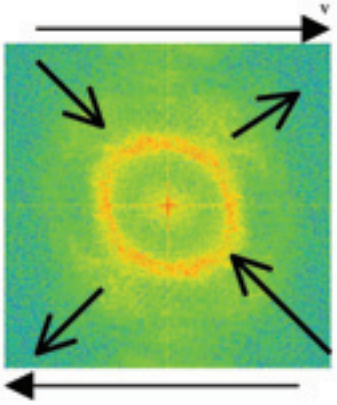

Schematic of the changes in the suspension microstructure as characterized by an FFT of an initially disordered suspension in the v–∇v plane at high Pe number. The arrows on the FFT indicate the compressional axis and the extensional axis of the flow field; the velocity vectors are drawn as well.

Familiar colloidal dispersions include paints, inks, cosmetics, pharmaceuticals and food. The macroscopic properties of suspensions are determined by the spatial organization of the particles, i.e. the microstructure.

J Vermant (Leuven) and M J Solomon (Michigan) review the sequences of structural states that can be induced in colloidal suspensions by the application of flow. Structure formation during flow is strongly affected by the delicate balance among interparticle forces, Brownian motion and hydrodynamic interactions. The resulting non-equilibrium microstructure determines the rheology. Colloidal suspensions with near hard-sphere interactions develop an anisotropic, amorphous structure at low dimensionless shear rates. At high rates, clustering due to strong hydrodynamic forces leads to shear thickening rheology.

Application of steady-shear flow to suspensions with repulsive interactions induces a rich sequence of transitions to one-, two- and three-dimensional order. Oscillatory-shear flow generates metastable ordering in suspensions with equilibrium liquid structure. However, short-range attractive interactions can lead to a fluid–gel transition under quiescent suspensions. Application of flow leads to orientation, break-up, densification and spatial reorganization of aggregates. Using a non-Newtonian suspending medium leads to additional possibilities for organization.

Vermant and Solomon examine the extent to which theory and simulation have yielded mechanistic understanding of the observed microstructural transitions. For fluid-like and ordered suspensions, the effects of flow are fairly well understood, and even quantitative predictive links between microstructure and macroscopic properties have been established. For weakly aggregated suspensions and for suspensions of particles in rheologically more complex fluids, more work is needed for mechanistic understanding. New experimental methods such as in situ CSLM microscopy and measurements on two-dimensional model suspensions may contribute to this development.

For numerical simulations, inclusion of hydrodynamic interactions helps develop understanding of the physical mechanisms involved and leads to prediction of macroscopic properties. Simulation methods that can accommodate either the non-ergodicity of aggregated suspensions or the non-Newtonian nature of the suspending media are difficult but necessary next steps.

Quantum phase transitions

Magnetic quantum phase transitions in Kondo lattices
Qimiao Si, Jian-Xin Zhu and D R Grempel
J. Phys.: Condens. Matter
17 (2005) R1025–R1040

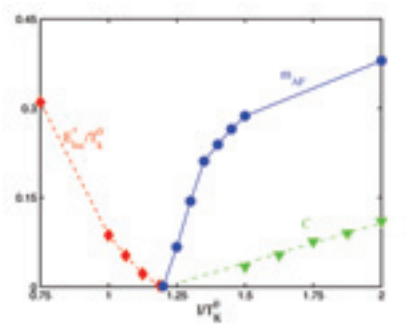

The coherence scale of the paramagnetic heavy fermion phase and the magnetic order parameter, m_{AF}, versus the tuning parameter, $\delta \equiv I/T_K^0$. Both quantities are determined at $T = 0.011\ T_K^0$. Also shown is the Curie constant of an unphysical solution without a magnetic order parameter at $\delta > \delta_c$. Lines are guides to the eye. The fact that all three curves meet at δ_c implies that the zero-temperature transition is continuous.

Heavy fermion systems, with quasiparticle mass over a hundred times the bare electron mass, are interesting for studying strongly correlated Fermi liquids and superconductors. The large mass reflects the Kondo screening of the magnetic moments, which is necessary to overcome magnetism. Heavy fermions are of interest for both experimental and theoretical studies of quantum critical points (QCP).

Magnetic QCP in heavy fermion metals are reviewed by Qimiao Si of Rice University and co-workers. The interplay between Kondo screening and magnetic interactions in Kondo lattice systems has been re-examined theoretically. A local quantum critical picture has emerged, in which magnetic interactions suppress Kondo screening precisely at the magnetic QCP. The Fermi surface undergoes a large reconstruction across the QCP and the coherence scale of the Kondo lattice vanishes there. The dynamical spin susceptibility exhibits ω/T scaling and non-trivial exponents describe the temperature and frequency dependences of various physical quantities, in contrast with the conventional spin density wave picture, in which the Kondo screening is not suppressed at the QCP and the Fermi surface evolves smoothly across the phase transition.

Si *et al* discuss recent microscopic studies of Kondo lattices within an extended dynamical mean field theory (EDMFT). Beyond the initial studies based on an M-expansion renormalization group method, Kondo lattice models with Ising anisotropy have been investigated, which have allowed the study of both the destruction of Kondo screening and the concomitant fractional exponent and ω/T scaling in the magnetic dynamics. They also discuss the magnetic phase diagram and summarize the evidence for the second-order nature of the magnetic quantum phase transition.

These microscopic approaches show that critical modes beyond the order parameter fluctuations exist associated with the destruction of Kondo screening. Consequences of this – in magnetic dynamics and also in the Fermi surface properties and thermodynamics – are supported by experiments. The insights will also help find a field theory that describes quantum critical heavy fermions, and they may be relevant to the exotic quantum critical behaviour in other strongly correlated systems such as doped Mott insulators.

Electrowetting

Electrowetting: from basics to applications
Frieder Mugele and Jean-Christophe Baret
J. Phys.: Condens. Matter
17 (2005) R705–R774

Contact line instability and emitted satellite droplets at high voltage. (Deionized water on silanized glass; droplet diameter: ≈3 mm.) Note the liquid necks between the satellites and the large droplet (inset).

Electrowetting is widely used to manipulate tiny amounts of liquids on surfaces in applications from 'lab-on-a-chip' devices to adjustable lenses and new kinds of electronic displays. Frieder Mugele and Jean-Christophe Baret of University of Twente review both fundamental and applied aspects of electrowetting.

The basis of electrowetting is a change of contact angle between an electrolyte and electrode on applying a voltage. In an external electric field, the charge carriers on the droplet surface of a conductive liquid redistribute, changing the surface morphology. The equilibrium surfaces remain surfaces of constant mean curvature because the electric field vanishes along the liquid–vapour interface, so capillarity determines the morphology. Electrowetting is then equivalent to conventional wetting on a surface with an identical distribution of local contact angles. This description is sufficient for most practical applications but breaks down under certain conditions.

Mugele and Baret compare the various approaches used to derive the basic electrowetting equation and discuss in detail the origin of the electrostatic forces that induce both contact angle reduction and the motion of entire droplets. They present some recent extensions to the theory accounting for distortions of the liquid surface by local electric fields, for the finite penetration depth of electric fields into the liquid, and for finite conductivity effects under an AC voltage. They also discuss the most prominent failure of the electrowetting equation, namely the saturation of the contact angle at high voltage, which recent work indicates is due to several distinct physical effects. With suitable electrode patterns or topographic structures on the substrate surface, variations of the contact angle can give rise not only to continuous changes of the droplet shape, but also to discontinuous morphological transitions between distinct liquid morphologies.

They briefly discuss the dynamics of electrowetting and finally give an overview of recent work aimed at commercial applications, in particular in the fields of adjustable lenses, display technology, fibre optics, and biotechnology-related microfluidic devices.

Moving molecules with the STM

Single-molecule manipulation and chemistry with the STM
N Lorente, R Rurali and H Tang
J. Phys.: Condens. Matter
17 (2005) S1049–S1074

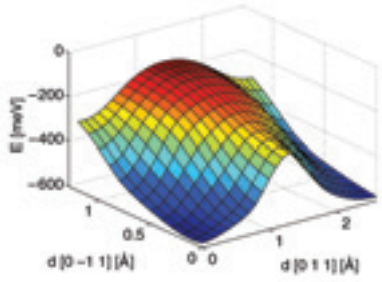

Potential energy surface of NH_3 along the Cu(100) surface calculated with the generalized gradient approximation using plane waves, and a 3×3 supercell where there is an ammonia molecule every three Cu atoms in the x and y directions of the surface. The plane axes are in Å, and the perpendicular axis in meV. The bridge side is at 1.29 Å along the [011] direction. It is a saddle point 301 meV in height. The hollow site of coordinates (1.29, 1.29) Å is a maximum. The barrier from top to hollow is 456 meV. The molecule needs less energy to go from top to top through the bridge site.

The scanning tunnelling microscope (STM) consists of a metallic tip, a tip manipulator and sophisticated electronics that record the tip–substrate electron current, bias voltage and manipulator motion. It is used to detect, analyse and modify adsorbed molecules.

N Lorente *et al* from Toulouse review single-adsorbate manipulation from a theoretical point of view. They review both mechanical manipulations, where the interaction exerted by the probe's tip on the adsorbate is used to initiate its motion, and recent work in the modelling and computation of inelastic effects localized at molecular adsorbates.

The aim is to account for the processes that permit controlled manipulation of matter at the atomic scale in adsorbed molecular systems. Simulations rely on total energy and electronic structure calculations where a trade-off is made between the size of the system and accuracy. This yields the basic quantities used for the next stage: the evaluation of the coupled electron–nuclear dynamics. This is a formidable task involving many approximations.

This review presents some of the customary approximations for the theoretical study of mechanical and inelastic manipulations. Mechanical manipulations use the interaction between the acting probe (usually a metallic tip) and the targeted adsorbate. The article reviews recent results in adsorbate mechanical manipulation and explains how manipulations can be effected by using the interaction between the probe's tip and certain molecular groups of complex chemisorbed molecular systems. On the other hand, inelastic manipulations use the tunnelling current to convey energy with sub-ångström precision. This current can excite localized vibrations that can induce measurable variations of the tunnelling conductance, hence providing a means of detecting single molecule vibrations. This current can also inject energy in a few reaction coordinates. Recently, the possibility of vibrational selective manipulations of NH_3/Cu(100) has been experimentally demonstrated. The theory presented here addresses the actual pathways accessed when the molecule is excited by the tunnelling current from an STM.

TiO_2 and ZnO for spintronics

Transition metal-doped TiO_2 and ZnO - present status of the field
Rebecca Janisch, Priya Gopal and Nicola A Spaldin
J. Phys.: Condens. Matter
17 (2005) R657–R689

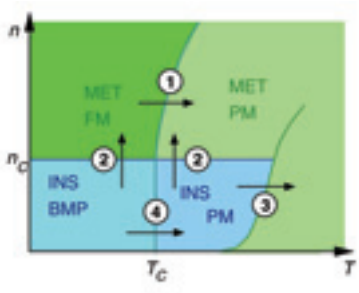

Schematic phase diagram of an oxygen-deficient semiconductor doped with magnetic impurities. Shown are the different phases as functions of carrier density n and temperature T. The bound magnetic polarons in the BMP phase can couple ferromagnetically. The marked transitions are: (1) the FM–PM transition in the metallic phase at T_C, (2) insulator–metal transitions as vacancies are screened for $n > n_C$, (3) the insulator–metal transition as electrons become thermally excited into the conduction band, and (4) transition from bound magnetic polarons to atomic paramagnetically ordered spins.

There is much current interest in 'spintronics' which uses the spin of electrons in addition to their charge in electronic devices. The study of spin-polarized transport also reveals new and fascinating fundamental physics in its own right.

Magnetic semiconductors are sought that will allow signal amplification and be compatible with standard semiconductor growth techniques. Of particular interest are the so-called diluted magnetic semiconductors (DMS) in which non-magnetic semiconductors are doped with magnetic atoms. DMS based on II–VI semiconductors such as CdTe or ZnSe have interesting magneto-optical properties but the magnetic interaction in II–VI semiconductors is dominated by the *anti*ferromagnetic exchange among the Mn spins and it is difficult to create p- or n-type carriers to mediate *ferro*magnetic interactions.

An important class of DMS is transition-metal-doped oxides. Co-doped TiO_2 is ferromagnetic with T_C up to 650 K reported. The origin of the ferromagnetic coupling is controversial but may result from the presence of Co clusters ($T_C \approx 1180$ K). Studies of ZnO doped with the whole range of 3d transition metal ions have variously shown high room-temperature ferromagnetism, spin-glass and paramagnetic behaviour.

Rebecca Janisch, Priya Gopal and Nicola Spaldin of University of California, Santa Barbara review the properties of Co-doped TiO_2, and Mn- and Co-doped ZnO to elucidate the origin and optimization of the magnetic properties. They also discuss the effect of other transition metal dopants, including V, Cr, Mn, Fe and Ni, in both oxides to compare the magnetism in ZnO- and TiO_2-based systems, and to evaluate the theoretical models for both.

They summarize the theoretical models that have been proposed to explain ferromagnetism in diluted magnetic semiconductors in general, and in oxide-based DMS in particular. Finally, they review the proposed mechanisms for the experimentally observed ferromagnetism and compare the predictions with the range of available data, outlining the experimental conditions that promote large magnetization and high ferromagnetic Curie temperature.

Surface roughness

On the nature of surface roughness with application to contact mechanics, sealing, rubber friction and adhesion

B N J Persson, O Albohr, U Tartaglino, A I Volokitin and E Tosatti

J. Phys.: Condens. Matter 17 (2005) R1–R62

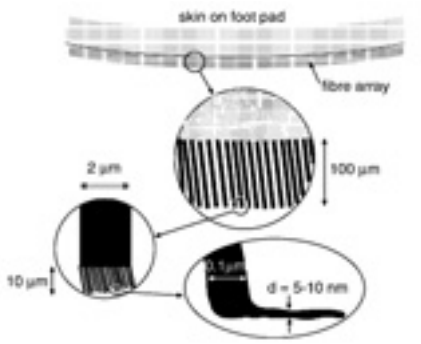

A schematic picture of the lizard adhesive system. The skin of the lizard is covered by a dense layer of thin fibres or hairs (setae; length: ≈100 μm and thickness of fibre: ~4 μm). Each of these fibres branches into about 1000 thinner fibres (length: ~10 μm and width: ~0.1 μm). Each of the thin fibres ends with a thin (5–10 nm) leaf-like plate (spatula).

B N J Persson (Jülich) and co-workers in Germany and Italy present a review of surface roughness, which has a huge influence on many common phenomena. It is the main reason why macroscopic bodies usually do not adhere to each other with any measurable strength.

As the size of a solid object decreases, its surface to volume ratio increases, so surface roughness becomes more important. Miniaturization of mechanical devices, e.g., microelectromechanical systems, requires a better understanding of the role of surface roughness in, e.g., contact mechanics and adhesion.

Surface roughness is also of great importance in many biological systems. Flies, bugs, crickets and lizards have very soft layers on their feet which allow them to attach and move on both very smooth and rough vertical solid walls. Another example is non-wetting coatings on plant surfaces based on surface roughness on many different length scales.

The roughness of surfaces can be studied over a wide length scale using optical methods (~1 μm to kilometers) and cantilever methods, e.g., the atomic force microscope (~1 nm to 100 μm). For randomly rough surfaces, the most important quantity is the surface roughness power spectrum. It determines the contact mechanics and adhesion for solid objects in direct contact, and also governs rubber friction on rough substrates, e.g., friction of tyres on a road surfaces, and influences other phenomena of technological importance, e.g., the roughness induced leaking of sealings.

The study of surface roughness is important for understanding many natural and biological phenomena and also for many technological processes. The present drive toward miniaturization and the design of optimal systems by transfer of ideas from biology to materials science, is likely to accelerate efforts to study and predict the influence of surface roughness on many phenomena.

Computing nanostructures

Carbon-based nanotechnology on a supercomputer

David Tománek

J. Phys.: Condens. Matter 17 (2005) R413–R459

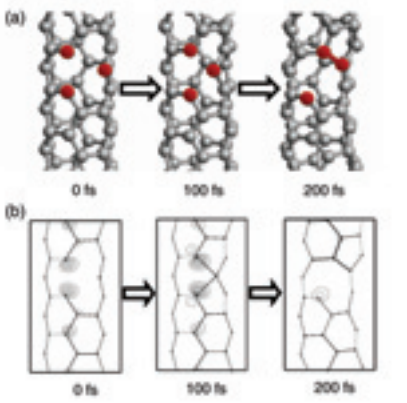

Self-healing process within a (3, 3) nanotube with a monatomic vacancy, induced by illumination. (a) Time evolution of the geometry. The three atoms adjacent to the vacancy and the new C–C bond, which forms ≈200 fs after the electronic excitation, are emphasized by colour and shading. (b) Time evolution of the partial charge density associated with the excited electron state. The lowest contour lines are common to the three panels.

Carbon nanostructures, particularly C_{60} and carbon nanotubes, are candidates for components of future nanoscale devices. They show unusual mechanical, thermal, electronic and optical properties.

The behaviour of these nanostructures is of essentially quantum nature. Since experimental observations are fundamentally influenced by the measurement itself, new approaches must be sought to design and test the future building blocks of nanotechnology, and large-scale computer simulations are indispensable to guide and complement the experiments. Addressing this challenge is imperative in view of the continuous reduction of device sizes, rapidly approaching the atomic level.

David Tománek of Michigan State University reviews some of the more intriguing phenomena associated with nanostructured carbon, including fullerenes, nanotubes and diamondoids.

Their unusual properties include the exceptionally high thermal conductance of nanotubes, a consequence of their quasi-1D structure, hard optical phonon frequencies, and large phonon mean free path. Trivalent carbon radicals may be sterically stabilized in specific sp_2 bonded carbon nanostructures, resulting in a net magnetization. Carbon nanotubes exhibit thermal contraction even well beyond room temperature, and may even be used as a nanoscale counterpart of a velcro bond. Nanotube peapods, formed by encapsulation of fullerenes or other molecules in nanotubes, emerge as intriguing nanostructures with many potential applications, including a computer memory or nanoscale chemical reactors. Fullerenes, nanotubes, and other sp_2 bonded carbon nanostructures may undergo large-scale morphological changes, including fusion, as a result of sequential Stone–Wales bond rotations. Defective nanotubes exhibit an unexpected self-healing ability at elevated temperatures and in the electronically excited state. Because of their unusually long lifetime, electronic excitations may be used to selectively remove oxygen impurities from nanotubes.